A Methodology to Investigate the Design Requirements of Plant Root-Inspired Robots for Soil Exploration

Serena R. M. Pirrone, Emanuela Del Dottore, Luc Sibille, and Barbara Mazzolai, *Member, IEEE*

***Abstract*—This letter proposes a methodology to investigate soil penetration requirements to extract specifications for designing robotic soil excavators and explorers. To this purpose, a three-dimensional (3-D) numerical model based on the Discrete Element Method (DEM) is proposed to simulate an intruder penetration and its interaction with the environment. In this study, the penetration process was analyzed as a function of the intruder diameter to median particle size ratio (Droot/D50), highlighting important differences for small and big ratios conditions (i.e., Droot/D50$<<$1 and Droot/D50$>>$1). In particular, the soil resistance force that autonomous penetration systems must overcome when moving into cohesionless granular soil was estimated based on the intruder size (diameter) and the median granularity (D50). This study estimates how the penetration requirements vary according to different penetration strategies. Specifically, a plant root-inspired axial movement emulating the growth from the tip adopted by plants is compared with a penetration obtained by pushing a system from the top. Our findings provide important guidelines about the design requirements (system size, penetration strategy, and actuation power) for artificial penetrating systems, like autonomous explorative robots, to improve their performances during underground exploration.**

***Index Terms*—Bioinspired robots, discrete numerical model, robot design requirements, robot-soil interaction, soil penetration.**

I. Introduction

CLASSICALLY adopted solutions for soil drilling and exploration still rely on cumbersome, energy-demanding, and intrusive technologies [1]. Current challenges include reducing the stresses exercised on the system, the energy expenditure, increasing the drilling system stabilization, providing steerability and branching to increase exploration of ample areas, and ensuring safety for the system, the operator, and the environment (e.g., reduction of vibrations, fuel leakage, soil removal) [2], [3]. In this context, robotics became a powerful tool to address these challenges [4], with bioinspired robots increasingly investigated in geotechnical engineering studies [4], [5]. The bioinspired approach aims to identify strategies of movement and exploration in living organisms that are relevant for improving the performance of artificial systems. In this process, the different spatial and temporal scales between living organisms and artificial systems and the different magnitudes of applied stresses and forces must be evaluated [5]. Various bioinspired burrowing robots were proposed for underground exploration [6]: a drill imitating the burrowing principle of wood wasp ovipositor [7], a robot mimicking the burrowing mechanism of razor clams [8], a sand crab-inspired robot [9], an inchworm-like robot [10], a marine worm inspired soft robot [11], and a robot mimicking the razor clam locomotion [12] are examples of animal-like robots. Despite their more recent breakthrough in bioinspired robotics compared to animals [13], plants also promise to suggest efficient strategies for soil penetration. Plant roots can inspire many exploratory solutions thanks to their ability to move efficiently under high stresses and soil constraints [14]. Various features of plant roots have been investigated with artificial robotic systems to evaluate their role in improving penetration performances, e.g., plant-like circumnutation movements [15], [16], sloughing and mucus-like mechanisms [17], [18], root tip-like morphology [19], and their indeterminate growth from the tip [20], [21]. The latter feature evolved as a new strategy of motion for robotic systems, favoring navigation in constrained environments, e.g., in soil [22], among obstacles [20], exploiting low-resistance pathways [23], [24]. Mazzolai et al. (2011) [25] proposed the first mechatronic system to mimic the apical part of plant roots and steers following gravity and moisture stimuli. In 2013, Sadeghi et al. [23] proposed the first concept of a skin-everting system, imitating roots sloughing cells lubricating mechanism and lateral hairs anchoring. A textile with embedded artificial hairs was everted from inside a shaft moving in granular media. The textile interface interposed between the shaft and the soil allowed the penetration force to drop by 30%. Later, the concept of growing from the tip adopted by plants to move was translated into a plant root-inspired robot capable of self-building its body through a layer-by-layer addition of new material just above the tip [22], [23] (Fig. 1). This mechanism consents the system to push forward its tip while keeping the growing body static with

Manuscript received 30 November 2022; accepted 9 April 2023. Date of publication 21 April 2023; date of current version 27 April 2023. This letter was recommended for publication by Associate Editor Z. Zhang and Editor X. Liu upon evaluation of the reviewers' comments. This work was supported by the European Research Council through the European Union's Horizon 2020 Research and Innovation Program under Grants 101003304 and I-WOOD. *(Corresponding authors: Serena R. M. Pirrone; Emanuela Del Dottore; Barbara Mazzolai.)*

Serena R. M. Pirrone is with the Istituto Italiano di Tecnologia, 16163 Genova, Italy, and also with Scuola Superiore Sant'Anna, The BioRobotics Institute, 56025 Pontedera, Pisa, Italy (e-mail: serena.pirrone@iit.it).

Emanuela Del Dottore is with the Istituto Italiano di Tecnologia, 16163 Genova, Italy (e-mail: emanuela.deldottore@iit.it).

Luc Sibille is with the Université Grenoble Alpes, CNRS, Grenoble INP, 3SR, F-38000 Grenoble, France (e-mail: luc.sibille@3sr-grenoble.fr).

Barbara Mazzolai is with the Istituto Italiano di Tecnologia, 16163 Genova, Italy (e-mail: barbara.mazzolai@iit.it).

Digital Object Identifier 10.1109/LRA.2023.3269318

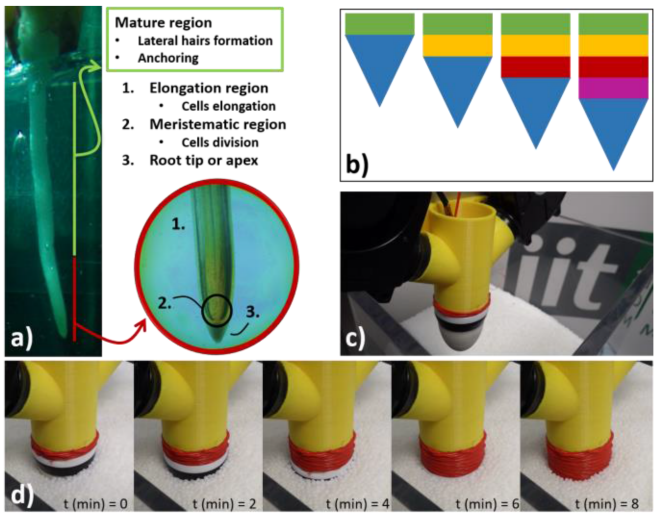

Fig. 1. (a) Zea mays root growing in agar medium with major zones depicted: mature region, where cells functionalize and the body remains static with respect to the environment, region of cell elongation where they axially elongate, meristematic region, where cells division occurs, and the root apex. (b) An abstraction of the growth process sketched over four successive steps: the tip is moved forward by the addition of a new layer (colored rectangles), as occurring with cells division. Previously added layers remain in their position, as occurring in mature region. (c) An example of growing robot. The robot implements the apical growth by an embedded additive manufacturing process by which a thermoplastic filament is heated and deposited circularly by the rotating tip [20], [22]. (d) A sequence of frames showing the progressive growth with the robot initiating penetration in a granular material.

respect to the environment allowing penetration into the soil with higher energy efficiency than a system that penetrates by being pushed externally from the top. Studying the interaction between soil and an intruder is of prominent importance to optimize the design of autonomous soil intruders and improve their penetration performances. This is a long-lasting problem that has been analyzed both experimentally, by considering penetrometers [26], [27], natural [15], [28], [29] and/or robotic roots [15], [16], and through mathematical models [14], [30]. Modeling soil penetration is highly challenging [31]. Several complex processes occur during soil interactions, such as the separation of soil layers, the appearance of cracks, and the flow of soil particles. Since processes involving large displacements and deformations cannot be modeled properly with finite element analysis, DEM numerical models [32], [33] were often preferred for modeling soil operations [34], [35], [36]. DEM-based models were used to analyze bioinspired burrowing strategies to extend the findings to engineering applications. For instance, Mishra et al. (2018) [19] evaluated both experimentally and through DEM numerical simulations how the penetration efficiency (in terms of penetration force) of a probe varies when a root-like tip morphology is considered rather than other geometries. In 2021, Chen et al. [32] used DEM simulations to model the self-penetration process of a bioinspired probe adopting an 'anchor-tip' burrowing strategy. This investigation analyzed how the probe geometry and the soil depth impact the ability of the probe to self-penetrate. In 2020, Pitcher et al. [37] proposed a bioinspired drilling system for space exploration combining the reciprocation motion of the wood wasp drill with a new oscillation motion mimicking the motion adopted by marine creatures to move in water and sandfish to bury in the sand. The authors investigated how the bit morphology affects drilling performances and proposed preliminary DEM simulations for analyzing multiple designs rapidly and provide information to experimental campaigns [37]. The authors later adopted DEM and multi-body dynamics (MBD) co-simulations to analyze different drilling methods and soil sampling, highlighting how penetration depth and contact forces depend on the tool–soil interactions [38], [39]. It is evident that numerical model-based analyses represent a key tool to evaluate, in combination with experimental campaigns, the performances of systems that operate in a certain environment and, therefore, to investigate their optimal design requirements.

This letter presents a three-dimensional (3-D) DEM-based numerical model used to simulate the penetration of a root-inspired digger into a cohesionless granular medium. The system penetrates the medium by growing axially from the tip and building its structure, whereas its upper structure remains fixed with the surrounding soil. In particular, this study investigates the penetration force the intruder must apply to explore the soil successfully. Force requirements are analyzed as a function of the system size (diameter, Droot) and soil granularity (median particle size, D50). Moreover, the estimated penetration pressure the root-like intruder needs to move into the soil is compared with the one needed by a system penetrating while being pushed from the top. The developed model can provide important guidelines on the intruder design specifications such as dimension, geometry, and actuation system requirements given soil specifications. In the following, the numerical model is presented (Section II), followed by the major outcomes (detailed in Section III) and the conclusion and future perspectives of this investigation (discussed in Section IV).

II. Methodology

The following 3-D DEM numerical model was developed using Yade [40]. Yade is an open-source framework comprising multiple functionalities to create DEM-based models and represent the physical properties of soils. This framework follows the classic approach proposed by Cundall and Strack (1979) [41], for which DEM simulates the mechanical behavior of a system composed of rigid bodies as a collection of discrete particles and a rigid intruder. The interactions among the particles are governed by physical laws computed using contact models [42] that consider the particles to interact in correspondence with a point of contact. After detecting the contacts, all forces acting on a particle are known, and the particle's position and orientation are computed using Newton's second law of motion [42]. DEM-based approaches assume that each particle can transmit the contact forces only to the close neighbor particles within the chosen time steps. These calculations are repeated until the system reaches the balance or once a pre-set simulation time is passed [42]. The soil model in Yade consists of discrete elements, referred to as particles, which may vary in shape, size, and mechanical properties. The particles may overlay and be merged to form a solid unit of any shape, referred to as a

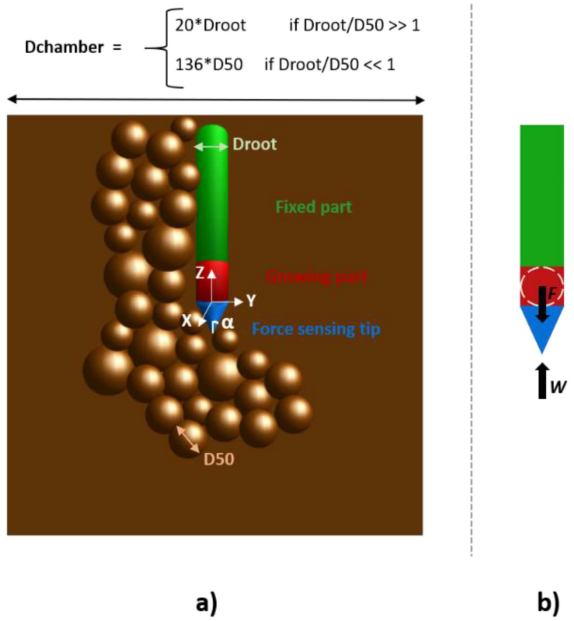

Fig. 2. (a) Scheme displaying the soil chamber, the root-like intruder and its regions of interest. (b) Scheme of force involved: the force F generated by the new added material (at the center of the body mass) that must counteract the vertical soil resistance W.

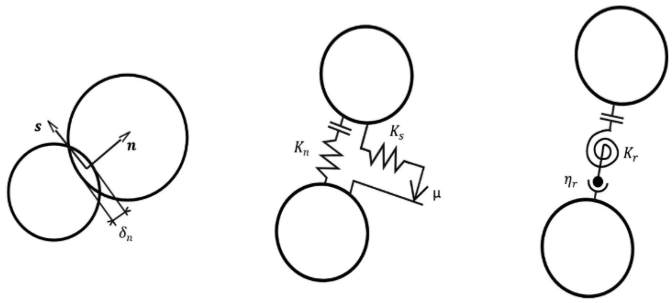

Fig. 3. Contact models used to model the inter-particle and the intruder-particles interactions. From left to right: overlapping of particles, friction model, and rolling model.

TABLE I
DEM INPUT PARAMETERS

Input parameter	Granular soil
Initial porosity	0.39
Stiffness modulus, [N m^{-2}]	$5 \cdot 10^8$
Shear to normal stiffness ratio	0.3
Rolling to shear stiffness ratio	5
Contact friction in deviatoric loading, [°]	19
Plastic rolling coefficient	0.55

clump. The software provides the possibility to represent an arbitrary shape as a packing of spheres, which follow a given size distribution; such packings are used to simulate soils [40] and bodies moving in it. Specifically, this numerical model considers a) a root-like intruder that consists of a cylindrical body with a diameter Droot and a conic tip with an aperture angle (2α) of 60°, b) a cubic chamber, with side Dchamber, made of 6 rigid and frictionless walls constituting the boundaries for the representative elementary volume (REV) of soil, c) a granular assembly (constituting the REV of soil) simulated by heterogeneously sized spherical particles characterized by a median particle size D50 (Fig. 2). As shown in Fig. 2, the cylindrical body includes three different regions: an upper region (in green) that represents the built body and is modeled as a single rigid body, a lower region (in red) that represents the region of growth, the newly added layer implemented through addition of new spherical particles with a diameter equal to the cylindrical body size Droot (and mostly overlaying the previous particles to conserve the cylindrical shape of this body), and a terminal conical part (in blue) that represents the apical tip that is pushed forward during growth. The inter-particles and intruder-particle interactions were modeled using an elastic, perfectly plastic contact model with dry friction and rolling resistance to counteract the rolling effect experienced by the virtual soil not evident in real granular media. Specifically, with respect to the contact plane between two spherical particles having radii R_1 and R_2, the normal $\boldsymbol{F_n}$ and shear (or tangential) $\boldsymbol{F_s}$ contact forces between the two spheres are expressed as in:

$$\boldsymbol{F_n} = K_n\, \delta_n \boldsymbol{n}. \tag{1}$$

$$\Delta \boldsymbol{F}_s = -K_s \Delta \boldsymbol{U}_s \text{ with } \|\boldsymbol{F}_s\| \leq \|\boldsymbol{F}_n\| tan\varphi_c. \tag{2}$$

where K_n and K_s are, respectively, the normal and tangential stiffnesses, φ_c represents the contact friction angle with a coefficient of contact friction $\mu = \tan\varphi_c$, $\boldsymbol{n}$ is the normal vector to the contact plane, δ_n is the overlap between the spheres, and $\boldsymbol{U_s}$ is the relative tangential displacement at the contact point. This law considers only compressive normal forces and the contact disappears when the overlap δ_n vanishes.

Considering that the rolling resistance at the contact is expressed through the rolling stiffness K_r and the coefficient of rolling friction η_r, the rolling moment $\boldsymbol{M_r}$ acting against the relative rolling rotation of particles θ_r is expressed as in:

$$\Delta \boldsymbol{M}_r = -K_r \Delta\theta_r \text{ with } \|\boldsymbol{M}_r\| \leq \|\boldsymbol{F}_n\| \eta_r \min(R_1,\ R_2)\,. \tag{3}$$

where $\Delta\theta_r$ represents the tangential component of the incremental relative rotation of the contacting spheres. Contact stiffnesses are defined as a function of stiffness modulus E_c, shear to normal stiffness ratio α_s and rolling to shear stiffness ratio α_r as expressed in:

$$K_n = 2E_c \frac{R_1 R_2}{R_1 + R_2};\ K_s = \alpha_s\, K_n;\ K_r = \alpha_r\, R_1 R_2 K_s. \tag{4}$$

This contact model does not include adhesive normal and tangential forces, thus simulating a cohesionless soil (e.g., fully dry sand on Earth). Fig. 3 shows a schematic of the contact models adopted to represent the inter-particle and intruder-particle interactions. Table I shows the DEM input parameters.

The intruder penetration simulation consists of two main steps: first, the packing is initialized by creating a loose, non-cohesive cloud of heterogeneously sized spheres, and then it is compacted under a confining pressure of 100 kPa in the triaxial directions; once the packing compaction is completed, the artificial root starts penetrating by growing axially from the tip. In

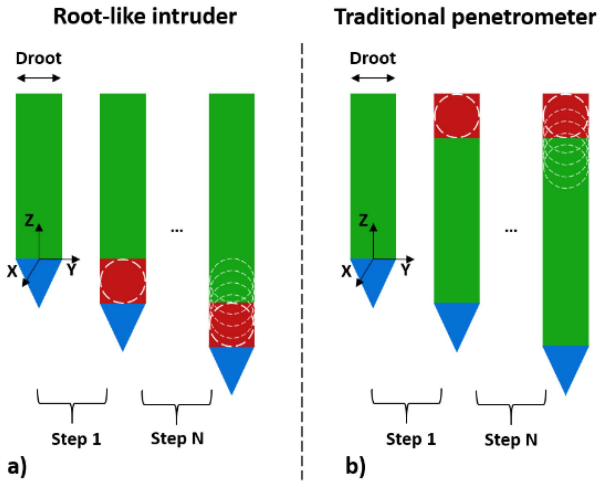

Fig. 4. Implementation used for modeling the penetration of a root-like intruder (a) and a penetrometer (b).

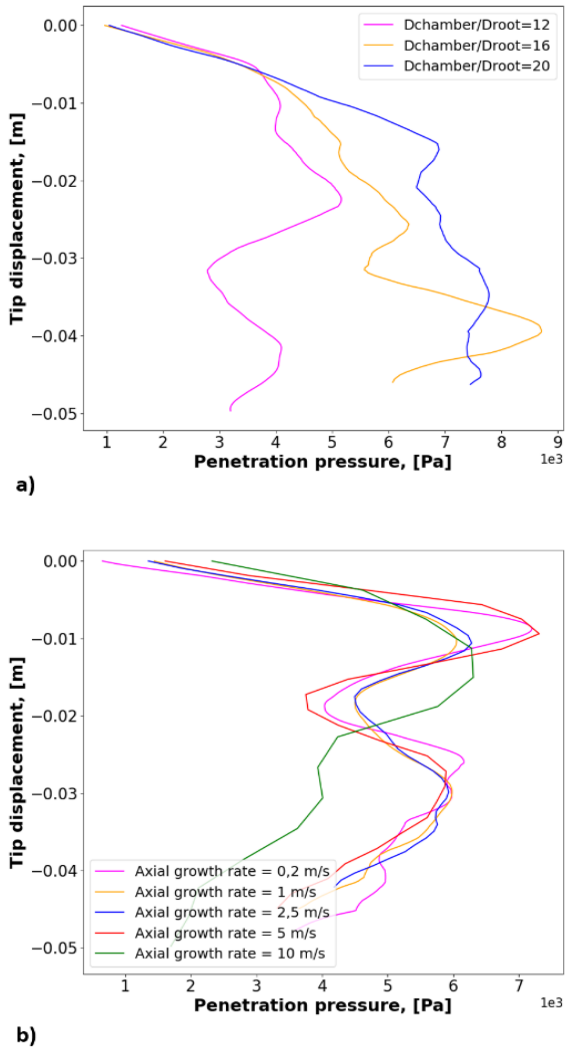

Fig. 5. (a) Outcomes of the Sensitivity Analysis conducted on 1) chamber to root size ratio (Dchamber/Droot) considering Droot/D50=6.8. (b) Root growth rate considering Droot/D50 = 6.8 and Dchamber/Droot = 20.

detail, the intruder axial growth process occurs as a sequence of discrete steps. Each growth step is implemented as follows (Fig. 4(a)): first, a sphere having a diameter Droot is added with the center located at a distance equal to Droot/2 from the top position of the tip; then, the sphere is moved along the z-axis by translational motion with an assigned constant velocity, pushing the tip forward. The axial forces perceived by the intruder during penetration were analyzed at steady-state conditions (i.e., when the average force reaches a mostly stable value) [43], [44]. These represent the expected working regime for the system, thus allowing extracting design specifications in terms of proper system diameter in relation to soil characteristics and the actuation power requirements. Following results reported in [16], where the steady-state condition was found approximately in the middle of the container height, the initial position of the intruder was set at the center (in x, y, and z) of the soil chamber. To reduce the boundary effects and to maintain computational efficiency, the relative dimensions of the soil chamber (Dchamber), soil particles (D50), and the intruder (Droot) are relevant [32], [33]. Thus, we conducted a Sensitivity Analysis (SA) on these parameters to define the working domain and the growth velocity. As shown in Fig. 2, the chamber size Dchamber varies with Droot/D50. For Droot/D50$>>$1, the ratio Dchamber/Droot = 20 represented an acceptable compromise to avoid boundary effects (because of reduced oscillations amplitude) and reduce computational time (Fig. 5(a)). For Droot/D50$<<$1, the chamber dimension is kept constant with a ratio of Dchamber/D50 = 136 to consider a realistic soil chamber size in all the case studies. For all analyzed case studies, the intruder's growth was set at 1 m/s, which is considered a threshold value below which the resisting force developed by the granular assembly on the intruder does not depend on the penetration velocity (Fig. 5(b)). In these conditions, the penetration force, or pressure, depends only on the mechanical properties of the contacts and the geometric arrangement of the particles. For higher penetration velocities, the penetration force may also be affected by the inertia of the soil particles and could be dependent on the penetration velocity itself. The latter corresponds to a dynamic regime which is not considered in this study. Besides, the soil is modeled as a discontinuous medium, i.e., composed of grains and voids. This results in scattered values of the penetration pressure around a stabilization value: while penetrating, the intruder tip perceives a soil resistance that decreases/increases when a void/grain is encountered. We analyzed the intruder penetration performances varying the system to median particle size ratio (Droot/D50) from 0.03 to 15. This analysis allows us to estimate a) how the soil resistance perceived by a penetration system (with a given size) depends on the considered medium granularities and, simultaneously, b) how the soil resistance perceived by intruders of different sizes during soil penetration (with a given granularity) depends on the intruder's dimension.

Performances are evaluated in terms of penetration pressures experienced only at the tip since, by the given definition of growth, the shaft does not slide over the soil particles (Fig. 2(b)). Finally, the penetration performances of the root-like intruder were compared with the performances of a system that penetrates by being pushed from the top (i.e., a traditional penetrometer).

This penetration process was modeled as a sequence of discrete steps too (Fig. 4(b)): in each penetration step, a new sphere is added at the top of the intruder shaft while pushing the shaft downward. As for the root-like intruder penetration modeling, the chamber-to-penetrometer size ratio and penetration velocity were set according to the SA. The penetrometer tip was initialized at the center (in x, y and z) of the soil chamber. By contrast to the root-like intruder penetration case, the penetration pressure requirements are estimated by considering the soil resistance on both the shaft and the tip.

III. Results

The axial soil resistance perceived by the root-like system was analyzed as a function of Droot/D50. Our findings show that the parameter Droot/D50 significantly affects the soil resistance behavior: the value around which the axial soil resistance force fluctuates rises with the increase of Droot/D50. When Droot/D50 $<<$ 1, the resistance forces exerted by the soil on the system during penetration tend to a value almost independent of Droot/D50. Indeed, by performing a linear regression and considering a confidence interval of 95%, we obtained a fitting line (the pink line in Fig. 6(a)) with slope (k):

$$k \;=\; 0.15 \pm 0.25. \tag{5}$$

By contrast, when Droot/D50 $>>$1, the soil resistance forces that the intruder needs to overcome follow a linearly increasing trend whose slope tends to 2 (blue dashed line in Fig. 6(a)). This result suggests that the forces for Droot/D50 $>>$1 depend proportionally on the square of the system diameter, implying soil resistance pressures that tend to a constant value, whatever Droot/D50 (Fig. 6(b)). This also recalls us about pile foundation theory [45], [46]. Pile foundations are adopted to transfer foundation loads to deeper soil strata that are stronger and less compressible. Soil resistance experienced by the pile in a cohesionless soil can be obtained by the formula [45], [46]:

$$q \;=\; a \cdot Nqmax, \tag{6}$$

where $a \;=\; 0.05\ MPa$ and $Nqmax$ is the bearing capacity factor, which is determined as a function of the internal friction angle of the soil [35]. In our case, considering an internal friction angle (φ) of 40° (the modeled soil has $\varphi \;=\; 38.1°$), eq. (6) produces a pile resistance of 17.75 MPa (the red line in Fig. 6(b)), in agreement with our simulation results (green triangles tend to align with the red line, Fig. 6(b)). This theoretical outcome thus validates the reliability of our model.

The histogram of the inter-particle contact forces in the whole particle packing and the related Probability Density Function (PDF) before the intruder starts the penetration is displayed in logarithmic scale in Fig. 7. During penetration, by testing Droot/D50 $=$ 0.03 and Droot/D50 $=$ 6.8, only the case Droot/D50 $=$ 0.03 (red line in Fig. 7) displayed an average tip-particle contact force (<Ftip>) within the range of particle-particle contact forces (Fparticles). This result suggests that the intruder behaves like a grain for a very small Droot/D50.

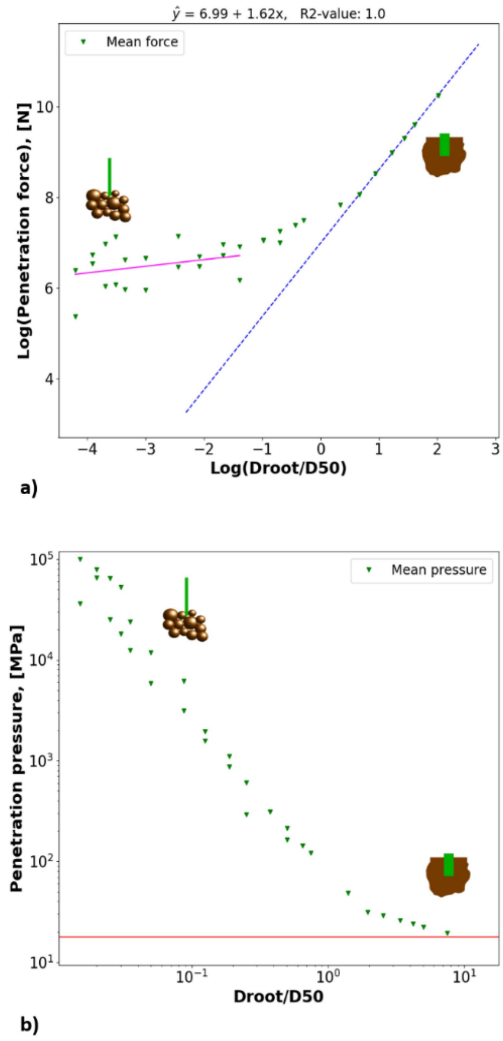

Fig. 6. Mean penetration force (a) and mean penetration pressure (b) dependence on the intruder size to median particle size ratio.

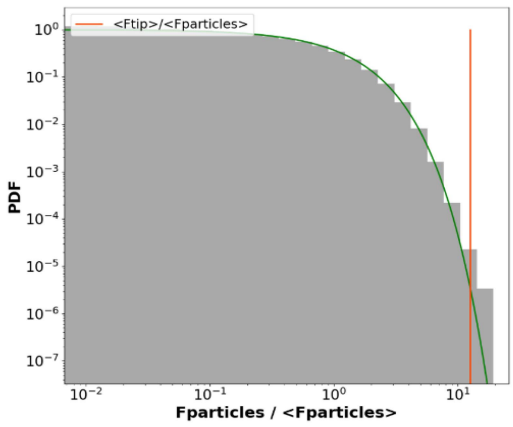

Fig. 7. Histogram of the inter-particle contact forces and the related PDF in logarithmic scale. The PDF is calculated from the inter-particle contact forces after the triaxial compression and before the intruder starts penetrating. <Fparticles> is the mean inter-particle force value, and <Ftip> is the mean tip-particles force value. The red line is the mean force value experienced by the tip during penetration, normalized on the inter-particle contact force mean value.

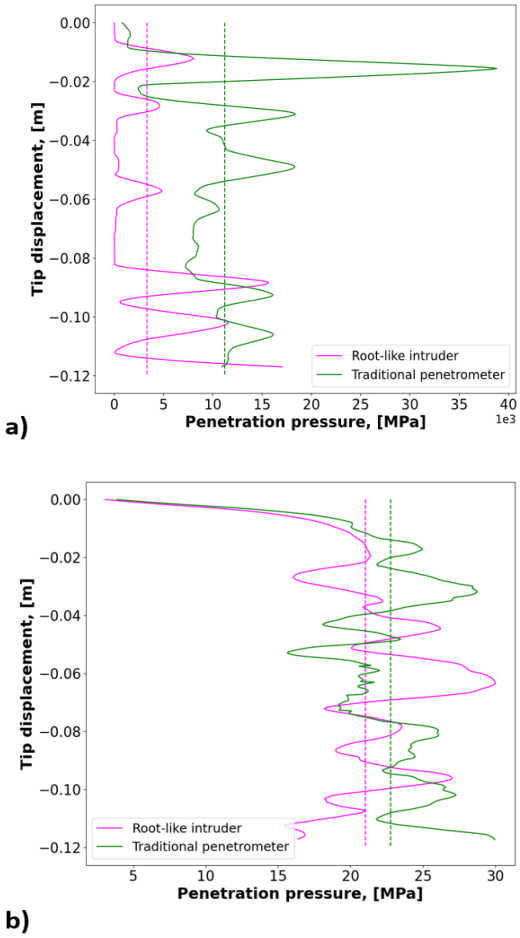

Fig. 8. Penetration pressure of a root-like intruder (in pink) compared to the actuation requirements of a traditional penetrometer (in green) for the cases Droot/D50 = 0.1 (a) and Droot/D50 = 6.8 (b).

Finally, the penetration performances of the root-like intruder were compared to those shown by a traditional penetrometer, i.e., penetration by means of apical growth vs. penetration by being pushed from the top. In order to investigate how the growth from the tip affects the system efficiency in underground exploration, this analysis was done for Droot/D50<<1 and Droot/D50>>1. Fig. 8(a) and (b) show the result for Droot/D50 = 0.1 and Droot/D50 = 6.8, respectively. In both conditions, the penetration performed by growing at the apical level is more beneficial in terms of actuation system requirements (less pressure experienced) than penetrating by being pushed from the top (Fig. 8). In particular, the advantage of implementing the growth from the tip is more relevant at small scales (small Droot/D50): respect to a traditional penetrometer, the pressure needed to be exerted by a root-like system to successfully penetrate drop by 70.4% when Droot/D50 = 0.1 (Fig. 8(a)), whereas it decreases by 7.7% when Droot/D50 = 6.8 (Fig. 8(b)). The different pressure variations may be found because, when the soil particles are much smaller than the intruder size (i.e., Droot/D50 = 6.8 case), there is much less opportunity to find a big pore where the system can move and, therefore, the system penetration is associated to the displacement of particles and soil compaction [14].

IV. Conclusion

This letter presents a 3-D DEM numerical model developed to simulate the penetration process into a cohesionless granular medium of a plant root-inspired system, i.e., a system that moves by apical growth. Specifically, the penetrating system implemented the growth process of plant roots employing the sequential addition of a section at the bottom of a cylindrical rod, pushing forward a conic tip and allowing penetration. The resistance exerted by the soil on the system is estimated to support the design of root-inspired soil explorative robots. Specifically, the model investigated the soil resistance forces that need to be considered to consent the axial propelling of the system. The study analyzed the performance as a function of the system tip dimension (Droot) and the soil granulometry (D50), considering the intruder size to median particle size ratio (Droot/D50) ranging between 0.03 and 15. This choice was made to develop a model capable of estimating the behavior of 1) a given system penetrating in diverse media possibly having different granularities and 2) systems having different sizes that penetrate a soil characterized by a certain granularity. Due to the heterogeneity of the medium, in all the analyzed cases, the penetration force experienced by the system shows fluctuations around a certain value, which rises with large Droot/D50 ratios. In particular, in conditions where Droot/D50>>1, our results show that the intruder tends to perceive a constant soil resistance pressure during penetration, which agrees with the expectations from pile foundation theory.

By contrast, when Droot/D50<<1, the system needs to overcome soil resistance forces that tend to a constant value. Furthermore, when very small ratios are analyzed (i.e., Droot/D50 = 0.03), our findings highlight that the intruder tip-particle and the inter-particle contact forces present similar values during the penetration process. This result suggests that when the intruder has a diameter smaller than the median soil particle size, it may be considered to behave as measuring the inter-particle forces. Furthermore, considering the different effects of Droot/D50 on the pressures, we compared the penetration performances of the root-like burrowing system with the performances of a traditional penetrometer, i.e., penetration by means of apical growth vs. penetration by pushing from the top. This analysis was done considering both cases with Droot/D50<<1 and Droot/D50>>1. Our results highlight that penetrating by growing at the apical level is always advantageous but with higher significance with small Droot/D50. The difference between the benefits in one and the other case may depend on the different intruder length-to-diameter ratios for big and small Droot/D50 values.

The model's confidence may be improved by widening the range of considered Droot/D50 ratios. Moreover, analyzing more data points within the range of 0.03<Droot/D50<15 may improve the resolution of the assessed case studies.

This study provides a methodology to support the design of artificial soil exploratory systems. By the proposed model, we can analyze and define important parameters, such as robot dimension, geometry, penetration strategies that can improve penetration, and actuation system requirements. As a future

perspective, this 3-D DEM numerical model may be employed to investigate how other penetration strategies adopted by plant roots (e.g., radial expansion and circumnutation movements) might affect the system penetration performances. Moreover, this numerical model could be used to simulate the penetration into soils with different mechanical properties (e.g., Martian or Lunar-like soils) in order to verify how the optimal design requirements vary when both terrestrial and space soil environments are considered.

Considering the prediction of the intruder penetration pressure requirements obtained through the numerical model, different actuation systems may be investigated to select the most accurate solution: based on the selected actuation system, this study may provide information on the maximum depth that the robot can achieve, therefore, enlighten the scenarios where the considered artificial system would perform better.

REFERENCES

[1] L. S. Blake, *Civil Engineer's Reference Book*, 4th ed. Burlington, VT, USA: Elsevier Science, 1989.

[2] E. I. Epelle and D. I. Gerogiorgis, "A review of technological advances and open challenges for oil and gas drilling systems engineering," *AIChE J.*, vol. 66, no. 4, Apr. 2020, doi: 10.1002/aic.16842.

[3] C. Simon, D. Goyallon, J.-P. Poloce, H. Sellami, L. Gerbaud, and A. Dourfaye, "Drilling without WOB: Dream or reality? An effective field test by total Angola," in *Proc. SPE/IADC Drilling Conf.*, 2007, Art. no. SPE-105522-MS, doi: 10.2118/105522-MS.

[4] K. M. Dorgan and K. A. Daltorio, "Fundamentals of burrowing in soft animals and robots," *Front. Robot. AI*, vol. 10, Jan. 2023, Art. no. 1057876, doi: 10.3389/frobt.2023.1057876.

[5] A. Martinez et al., "Bio-inspired geotechnical engineering: Principles, current work, opportunities and challenges," *Géotechnique*, vol. 72, pp. 687–705, May 2021, doi: 10.1680/jgeot.20.P.170.

[6] H. Wei et al., "Review on bioinspired planetary regolith-burrowing robots," *Space Sci. Rev.*, vol. 217, no. 8, Dec. 2021, Art. no. 87, doi: 10.1007/s11214-021-00863-2.

[7] Y. Gao, A. Ellery, M. Jaddou, J. Vincent, and S. Eckersley, "A novel penetration system for *in situ* astrobiological studies," *Int. J. Adv. Robot. Syst.*, vol. 2, no. 4, Dec. 2005, Art. no. 29, doi: 10.5772/5779.

[8] A. G. Winter, R. L. H. Deits, D. S. Dorsch, A. E. Hosoi, and A. H. Slocum, "Teaching RoboClam to dig: The design, testing, and genetic algorithm optimization of a biomimetic robot," in *Proc. IEEE/RSJ Int. Conf. Intell. Robots Syst.*, 2010, pp. 4231–4235, doi: 10.1109/IROS.2010.5654364.

[9] R. A. Russell, "CRABOT: A biomimetic burrowing robot designed for underground chemical source location," *Adv. Robot.*, vol. 25, no. 1–2, pp. 119–134, Jan. 2011, doi: 10.1163/016918610X538516.

[10] T. Dewei, Z. Weiwei, J. Shengyuan, S. Yi, and C. Huazhi, "Development of an inchworm boring robot(IBR) for planetary subsurface exploration," in *Proc. IEEE Int. Conf. Robot. Biomimetics*, 2015, pp. 2109–2114, doi: 10.1109/ROBIO.2015.7419085.

[11] D. Ortiz, N. Gravish, and M. T. Tolley, "Soft robot actuation strategies for locomotion in granular substrates," *IEEE Robot. Autom. Lett.*, vol. 4, no. 3, pp. 2630–2636, Jul. 2019, doi: 10.1109/LRA.2019.2911844.

[12] J. Tao, S. Huang, and Y. Tang, "SBOR: A minimalistic soft self-burrowing-out robot inspired by razor clams," *Bioinspiration Biomimetics*, vol. 15, no. 5, Jul. 2020, Art. no. 055003, doi: 10.1088/1748-3190/ab8754.

[13] B. Mazzolai, L. Beccai, and V. Mattoli, "Plants as model in biomimetics and biorobotics: New perspectives," *Front. Bioeng. Biotechnol.*, vol. 2, 2014, Art. no. 2.

[14] E. Kolb, V. Legué, and M.-B. Bogeat-Triboulot, "Physical root—Soil interactions," *Phys. Biol.*, vol. 14, no. 6, Nov. 2017, Art. no. 065004, doi: 10.1088/1478-3975/aa90dd.

[15] E. Del Dottore, A. Mondini, A. Sadeghi, V. Mattoli, and B. Mazzolai, "Circumnutations as a penetration strategy in a plant-root-inspired robot," in *Proc. IEEE Int. Conf. Robot. Automat.*, 2016, pp. 4722–4728, doi: 10.1109/ICRA.2016.7487673.

[16] E. Del Dottore, A. Mondini, A. Sadeghi, V. Mattoli, and B. Mazzolai, "An efficient soil penetration strategy for explorative robots inspired by plant root circumnutation movements," *Bioinspiration Biomimetics*, vol. 13, no. 1, Dec. 2017, Art. no. 015003, doi: 10.1088/1748-3190/aa9998.

[17] A. Sadeghi, A. Tonazzini, L. Popova, and B. Mazzolai, "Robotic mechanism for soil penetration inspired by plant root," in *Proc. IEEE Int. Conf. Robot. Automat.*, 2013, pp. 3457–3462, doi: 10.1109/ICRA.2013.6631060.

[18] A. K. Mishra, F. Tramacere, and B. Mazzolai, "From plant root's sloughing and radial expansion mechanisms to a soft probe for soil exploration," in *Proc. IEEE Int. Conf. Soft Robot.*, 2018, pp. 71–76, doi: 10.1109/ROBOSOFT.2018.8404899.

[19] A. K. Mishra, F. Tramacere, R. Guarino, N. M. Pugno, and B. Mazzolai, "A study on plant root apex morphology as a model for soft robots moving in soil," *Plos One*, vol. 13, no. 6, Jun. 2018, Art. no. e0197411, doi: 10.1371/journal.pone.0197411.

[20] A. Sadeghi, E. Del Dottore, A. Mondini, and B. Mazzolai, "Passive morphological adaptation for obstacle avoidance in a self-growing robot produced by additive manufacturing," *Soft Robot.*, vol. 7, no. 1, pp. 85–94, Feb. 2020, doi: 10.1089/soro.2019.0025.

[21] N. D. Naclerio et al., "Controlling subterranean forces enables a fast, steerable, burrowing soft robot," *Sci. Robot.*, vol. 6, Jun. 2021, Art. no. 55, doi: 10.1126/scirobotics.abe2922.

[22] A. Sadeghi, A. Mondini, and B. Mazzolai, "Toward self-growing soft robots inspired by plant roots and based on additive manufacturing technologies," *Soft Robot.*, vol. 4, no. 3, pp. 211–223, Sep. 2017, doi: 10.1089/soro.2016.0080.

[23] A. Sadeghi, A. Tonazzini, L. Popova, and B. Mazzolai, "A novel growing device inspired by plant root soil penetration behaviors," *Plos One*, vol. 9, no. 2, Feb. 2014, doi: 10.1371/journal.pone.0090139.

[24] A. Tonazzini, A. Sadeghi, L. Popova, and B. Mazzolai, "Plant root strategies for robotic soil penetration," in *Biomimetic and Biohybrid Systems*, vol. 8064, N. F. Lepora, A. Mura, H. G. Krapp, P. F. M. J. Verschure, and T. J. Prescott, Eds., Berlin, Germany: Springer, 2013, pp. 447–449, doi: 10.1007/978-3-642-39802-5_62.

[25] B. Mazzolai et al., "A miniaturized mechatronic system inspired by plant roots for soil exploration," *IEEEASME Trans. Mechatron.*, vol. 16, no. 2, pp. 201–212, Apr. 2011, doi: 10.1109/TMECH.2009.2038997.

[26] A. G. Bengough and C. E. Mullins, "Mechanical impedance to root growth: A review of experimental techniques and root growth responses," *J. Soil Sci.*, vol. 41, no. 3, pp. 341–358, Sep. 1990, doi: 10.1111/j.1365-2389.1990.tb00070.x.

[27] A. G. Bengough, C. E. Mullins, G. Wilson, and J. Wallace, "The design, construction and use of a rotating-tip penetrometer," *J. Agricultural Eng. Res.*, vol. 48, pp. 223–227, Jan. 1991, doi: 10.1016/0021-8634(91)80017-9.

[28] F. Migliaccio, A. Fortunati, and P. Tassone, "Arabidopsis root growth movements and their symmetry: Progress and problems arising from recent work," *Plant Signal. Behav.*, vol. 4, no. 3, pp. 183–190, Mar. 2009, doi: 10.4161/psb.4.3.7959.

[29] J. Yan, B. Wang, and Y. Zhou, "A root penetration model of arabidopsis thaliana in phytagel medium with different strength," *J. Plant Res.*, vol. 130, no. 5, pp. 941–950, Sep. 2017, doi: 10.1007/s10265-017-0926-4.

[30] F. Tedone, E. Del Dottore, M. Palladino, B. Mazzolai, and P. Marcati, "Optimal control of plant root tip dynamics in soil," *Bioinspiration Biomimetics*, vol. 15, no. 5, Sep. 2020, Art. no. 056006, doi: 10.1088/1748-3190/ab9a15.

[31] S. R. M. Pirrone, E. Del Dottore, and B. Mazzolai, "Historical evolution and new trends for soil-intruder interaction modeling," *Bioinspiration Biomimetics*, vol. 18, no. 1, Nov. 2022, Art. no. 011001, doi: 10.1088/1748-3190/ac99c4.

[32] Y. Chen, A. Khosravi, A. Martinez, and J. DeJong, "Modeling the self-penetration process of a bio-inspired probe in granular soils," *Bioinspiration Biomimetics*, vol. 16, no. 4, Jul. 2021, Art. no. 046012, doi: 10.1088/1748-3190/abf46e.

[33] A. Khosravi, A. Martinez, and J. T. DeJong, "Discrete element model (DEM) simulations of cone penetration test (CPT) measurements and soil classification," *Can. Geotechnical J.*, vol. 57, no. 9, pp. 1369–1387, Sep. 2020, doi: 10.1139/cgj-2019-0512.

[34] Z. Asaf, D. Rubinstein, and I. Shmulevich, "Determination of discrete element model parameters required for soil tillage," *Soil Tillage Res.*, vol. 92, no. 1–2, pp. 227–242, Jan. 2007, doi: 10.1016/j.still.2006.03.006.

[35] I. Shmulevich, "State of the art modeling of soil–tillage interaction using discrete element method," *Soil Tillage Res.*, vol. 111, no. 1, pp. 41–53, Dec. 2010, doi: 10.1016/j.still.2010.08.003.

[36] C. Plouffe, C. Laguë, S. Tessier, M. J. Richard, and N. B. McLaughlin, "Moldboard plow performance in a clay soil: Simulations and experiment," *Trans. ASAE*, vol. 42, no. 6, pp. 1531–1540, 1999, doi: 10.13031/2013.13317.

[37] C. Pitcher, M. Alkalla, X. Pang, and Y. Gao, "Development of the third generation of the dual-reciprocating drill," *Biomimetics*, vol. 5, no. 3, Aug. 2020, Art. no. 38, doi: 10.3390/biomimetics5030038.

[38] M. Alkalla, X. Pang, C. Pitcher, and Y. Gao, "DROD: A hybrid biomimetic undulatory and reciprocatory drill: Quantitative analysis and numerical study," *Acta Astronaut.*, vol. 182, pp. 131–143, May 2021, doi: 10.1016/j.actaastro.2021.02.007.

[39] C. Pitcher, X. Pang, M. Alkalla, and Y. Gao, "Development of a multi-sample acquisition technique for efficient planetary subsurface exploration," *Acta Astronaut.*, vol. 198, pp. 309–319, Sep. 2022, doi: 10.1016/j.actaastro.2022.06.008.

[40] V. Šmilauer et al., "Yade documentation," 3rd ed. The Yade Project, 2021, doi: 10.5281/zenodo.5705394.

[41] P. A. Cundall and O. D. L. Strack, "A discrete numerical model for granular assemblies," *Géotechnique*, vol. 29, no. 1, pp. 47–65, Mar. 1979, doi: 10.1680/geot.1979.29.1.47.

[42] M. Ucgul, J. M. Fielke, and C. Saunders, "Three-dimensional discrete element modelling of tillage: Determination of a suitable contact model and parameters for a cohesionless soil," *Biosyst. Eng.*, vol. 121, pp. 105–117, May 2014, doi: 10.1016/j.biosystemseng.2014.02.005.

[43] M. Bolton, M. Gui, J. Garnier, G. Bagge, L. Laue, and R. Renzi, "Centrifuge cone penetration tests in sand," *Géotechnique*, vol. 49, no. 4, pp. 543–552, 1999.

[44] W. Huang, D. Sheng, S. Sloan, and H. Yu, "Finite element analysis of cone penetration in cohesionless soil," *Comput. Geotech.*, vol. 31, no. 7, pp. 517–528, 2004.

[45] H. H. Tamboura, K. Isobe, and S. Ohtsuka, "End bearing capacity of a single incompletely end-supported pile based on the rigid plastic finite element method with non-linear strength property against confining stress," *Soils Found.*, vol. 62, no. 4, Aug. 2022, Art. no. 101182, doi: 10.1016/j.sandf.2022.101182.

[46] G. G. Meyerhof, "Bearing capacity and settlement of pile foundations," *J. Geotechnical Eng. Division*, vol. 102, no. 3, pp. 197–228, Mar. 1976, doi: 10.1061/AJGEB6.0000243.

Open Access funding provided by 'Istituto Italiano di Tecnologia' within the CRUI CARE Agreement